IEEE Access
Multidisciplinary ⋮ Rapid Review ⋮ Open Access Journal

Received March 23, 2022, accepted April 3, 2022, date of publication April 7, 2022, date of current version April 21, 2022.

Digital Object Identifier 10.1109/ACCESS.2022.3165589

Modeling Dispersive Media in Finite-Difference Time-Domain Method for Radiative Cooling Applications

MUNSEONG BAE[1,2] AND HAEJUN CHUNG[1]
[1]School of Electrical Engineering, Soongsil University, Seoul 06978, South Korea
[2]Department of Mechanical Engineering, Massachusetts Institute of Technology, Cambridge, MA 02139, USA

Corresponding author: Haejun Chung (haejun@ssu.ac.kr)

This work was supported by the Soongsil University Research Fund (New Professor Support Research) of 2021.

ABSTRACT Radiative cooling offers a new strategy to address building cooling problems in an environmentally friendly way, compared with traditional cooling methods that require high-power consumption. The goal of radiative cooling is to maximize absorption at the mid-infrared (MIR) spectrum (8–13μm). Thus, it is important to characterize the dispersive relationship of the radiative cooling materials (TiO_2, Si_3N_4, SiC, SiO_2) in the MIR regime. In this work, we use the multi-pole Lorentz dispersion equation to model frequency-dependent dielectric constants of radiative cooling materials, which requires particle swarm optimization to solve multidimension optimization problems. This modeling can be directly applicable to the auxiliary differential equation (ADE)-based finite-difference time-domain (FDTD) method for simulating emissivity of radiative cooling materials. Further, we limit the number of Lorentz poles to five, which minimizes the computational burden in ADE–FDTD. Then, we validate our FDTD results against an analytic prediction calculated by the transfer matrix method. Finally, we demonstrate a highly efficient radiative cooling structure based on a simple SiO_2 grating. The proposed material modeling can accelerate the nano/microstructural design of the radiative cooling strategies.

INDEX TERMS Finite-difference time-domain (FDTD) method, particle swarm optimization (PSO), Lorentz dispersion model.

I. INTRODUCTION

Radiative cooling offers a new strategy to address photovoltaic and building cooling problems in an environmentally friendly way. Traditional cooling methods require power consumption with external devices, which occupy a large portion of energy consumption in everyday life. On the other hand, passive cooling methods are broadly classified as bio-inspired cooling strategies [1]–[4] and artificial structure-based strategies [5], [6], both reflecting the solar spectrum while maximizing absorption in the mid-infrared (MIR) spectrum (8–13μm).

In this MIR spectrum, strong selective thermal emission reaches the unlimited cold heat sink of space ($\sim$ 3K), utilizing a transparency window of the Earth's atmosphere where the radiation absorption is insignificant. A recent advance of nano-fabrication has been applied to daytime radiative cooling applications such as metamaterials [7]–[9], polymers [7], [10], [11], and photonic structures [12]–[14]. In order to further improve radiative cooling performance, it is essential to precisely engineer radiative cooling materials with advanced nano/microstructures [12], [15]. This brings challenges to numerical simulations of the radiative cooling materials. For example, rigorous-coupled-wave analysis (RCWA)) [16], [17], discrete dipole approximation (DDA) [18], and the transfer matrix method (TMM) [19], [20] can be used to solve photonic structures relatively fast. However, they are not preferable for studying complicated (or enormous) structures due to assumptions on their methods [21], [22]. On the other hand, solving full-wave Maxwell's equations provides accurate solutions, wherein the most representative examples of full-wave Maxwell solvers are the finite element method (FEM) [23], [24] or FDTD [11], [25]. The former utilizes unstructured mesh with steady-state analysis, which makes it powerful for analyzing accurate solutions for complex 3D geometries in discrete frequencies.

The associate editor coordinating the review of this manuscript and approving it for publication was Guido Lombardi.

This work is licensed under a Creative Commons Attribution 4.0 License. For more information, see https://creativecommons.org/licenses/by/4.0/

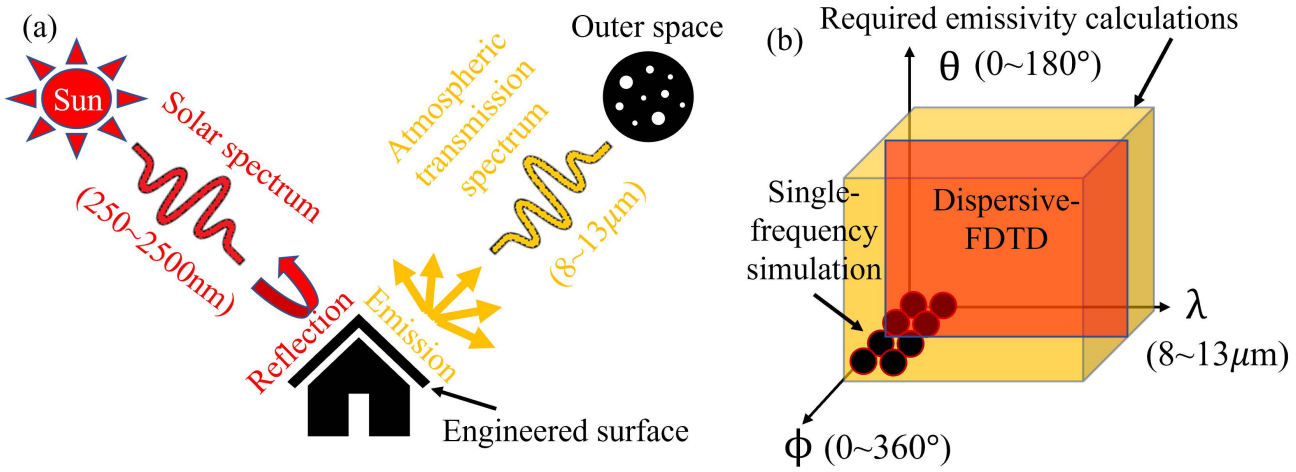


FIGURE 1. (a) A schematic diagram of the radiative cooling process for building structures. The engineered surface fully reflects the solar spectrum while emissivity at the atmospheric transmission spectrum is maximized. (b) The yellow volume indicates required emissivity calculations for studying radiative cooling applications. The black spheres indicate an emissivity covered by one single frequency simulation. The orange area indicates an example of emissivity covered by one simulation of dispersive FDTD. Well-developed dispersive FDTD can accelerate radiative cooling simulations significantly.

However, the nature of steady-state analysis in FEM requires multiple simulations to obtain a broadband response of photonic structures. The latter solves the differential form of Maxwell equations over time and space. It employs a staircase mesh, which is known as Yee's grid. This offers potential for efficient parallelization in multicore computing. Also, the time-domain response obtained by a single simulation in FDTD can be easily converted to a broadband frequency response by Fourier transformation [22], [26]–[28] as shown in Fig. 1(b) (orange area). The main hurdle on using FDTD for a radiative cooling study is modeling dispersive materials for the MIR regime. The FDTD method requires converting frequency-dependent material parameters to an auxiliary time-domain differential equation for simulating dispersive materials [22].

In this work, we use the Lorentz dispersion model to fit the frequency-dependent dielectric constants of the radiative cooling materials via particle swarm optimization (PSO) [29]–[31]. The Lorentz dispersion equation, also known as the Drude–Lorentz oscillator model, involves modeling electrons as a damped harmonic oscillator. By superposing multiple Lorentz equations, we can efficiently model arbitrary frequency-dependent permittivities of the radiative cooling materials for FDTD simulations. A single Lorentz equation has plasma frequency, resonance frequency, and damping coefficient as its parameters, which can be fitted using the least-squares method [32] or others [33]–[37], while fitting parameters for multipole Lorentz equations is more challenging. Therefore, finding a fewer pole dispersion model that can fit the experimental complex permittivity data is significant, guaranteeing faster and memory-efficient FDTD simulations. We apply a new figure of merit to the PSO method to discover the Lorentz parameters in this work. Then, we compare our method against a conventional PSO method and genetic algorithm. Additionally, we compare dispersive FDTD simulations against analytic calculations based on the transfer matrix method (TMM) [19], [38] for broad angles and broadband to validate our result. This study may facilitate a realization of novel radiative cooling design by enabling faster and accurate simulations of the radiative cooling materials.

II. MULTI-POLE LORENTZ MODEL OF RADIATIVE COOLING MATERIALS

The ADE approach can be applied to simulate Lorentz dispersion materials [39], [40] and many others [41]–[43] in FDTD [22]. The Lorentz model is written as

$$\varepsilon_{\mathrm{r}}(\omega) = \varepsilon_{\infty} + \sum_{n} \frac{\Delta\varepsilon_{\mathrm{n}} \cdot \omega_{\mathrm{n}}^2}{\omega_{\mathrm{n}}^2 - \omega^2 + j\omega\gamma_{\mathrm{n}}}, \tag{1}$$

where ε_{r} is relative permittivity, ε_{∞} is a constant offset for the real part of the dielectric function, n is the number of pole, $\Delta\varepsilon_{\mathrm{n}}$ is a relative value of the plasma frequency compared to the resonance frequency, γ_{n} is damping coefficient, and ω_{n} is the resonance frequency of the oscillator. The second term denotes Lorentz oscillator model with n_{th} poles. Then, frequency-domain Maxwell's equations can be written as

$$\nabla \times H = j\omega\varepsilon_0\varepsilon_{\mathrm{r}}(\omega)E \tag{2}$$

$$\nabla \times E = -j\omega\mu_0\mu_{\mathrm{r}}B. \tag{3}$$

After inserting Lorentz model (Eq. 1) into Eq. 2, the Maxwell's equations become

$$\nabla \times H = j\omega\varepsilon_0 \left(\varepsilon_{\infty} + \sum_{n} \frac{\Delta\varepsilon_{\mathrm{n}} \cdot \omega_{\mathrm{n}}^2}{\omega_{\mathrm{n}}^2 - \omega^2 + j\omega\gamma_{\mathrm{n}}}\right) E. \tag{4}$$

It can be simplified to

$$\left(\sum_{n} \frac{\Delta\varepsilon_{\mathrm{n}} \cdot \omega_{\mathrm{n}}^2}{\omega_{\mathrm{n}}^2 - \omega^2 + j\omega\gamma_{\mathrm{n}}}\right) E = P_{\mathrm{L}}, \tag{5}$$

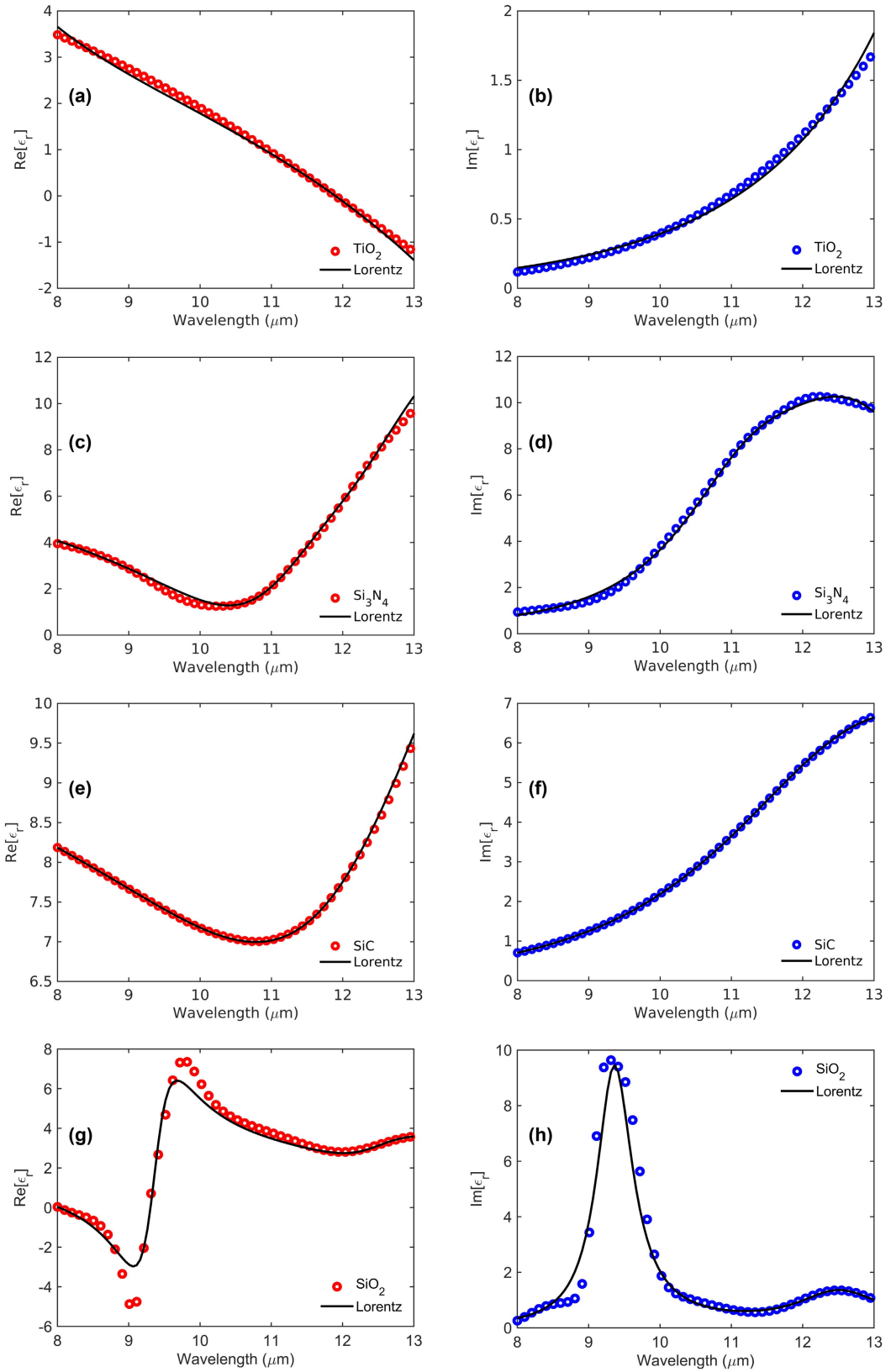


FIGURE 2. Complex curve fitting of dispersive materials using the multi-pole Lorentz model. The solid lines and symbols indicate the results of the Lorentz model and the experimental data (TiO_2 [44], Si_3N_4 [44], SiC [45], SiO_2 [46], [47]) of dispersive material, respectively. The real part of relative permittivities of TiO_2 (a), Si_3N_4 (c), SiC (e), SiO_2 (g). The imaginary part of relative permittivities of TiO_2 (b), Si_3N_4 (d), SiC (f), SiO_2 (h).

TABLE 1. Lorentz parameters for each material obtained by the proposed PSO algorithm. The unit of Lorentz parameter is 'a/c' where 'a' is 10μm and 'c' is a speed of light where Meep [48] defines it as 1 to fully utilize scale invariant characteristic of Maxwell's equation.

Material	Parameters [a/c]	pole 1	pole 2	pole 3	pole 4	pole 5
TiO_2 (5 pole)	ω_n	0.579635	0.002740	0.000563	1.991540	1.790816
	γ_n	0.128380	8.085622	5.587462	15.208301	0.000000
	$\Delta\varepsilon_n$	4.172449	12.142995	3.477039	0.000000	1.938847
Si_3N_4 (5 pole)	ω_n	3.779706	0.784682	0.886019	2.661516	1.540996
	γ_n	0.058024	0.182981	0.218751	2.869409	8.007411
	$\Delta\varepsilon_n$	4.597450	1.578285	1.397234	0.151951	0.040598
SiC (5 pole)	ω_n	13.627142	0.000078	15.306823	0.767414	0.000027
	γ_n	0.000000	21.766770	0.000000	0.355457	15.097573
	$\Delta\varepsilon_n$	2.211264	3.174987	6.453698	3.083026	10.966395
SiO_2 (4 pole)	ω_n	1.376351	0.799733	37.554292	1.068543	
	γ_n	8.337983	0.094954	2.467970	0.070044	NA
	$\Delta\varepsilon_n$	0.010231	0.143004	0.740878	0.617576	

TABLE 2. The quality of our fitting against the most widely used evolutionary algorithms (conventional genetic algorithm, conventional particle swarm optimization). We assume that the conventional PSO and the conventional GA algorithms have a figure of merit (F) given by $\mathcal{F} = \sum_\omega \frac{[\varepsilon_{\text{Dat.}}(\omega) - \varepsilon_{\text{Lorentz}}(\omega)]}{[\varepsilon_{\text{Lorentz}}(\omega)]}$.

Fitting error (RMS)	Conventional PSO [29]	PSO with real and imaginary	Conventional GA [49]	Our PSO
TiO_2 (5 pole)	31.44	31.66	92.82	9.82
Si_3N_4 (5 pole)	13.22	13.65	51.11	4.62
SiC (5 pole)	0.32	0.38	25.22	0.31
SiO_2 (4 pole)	54.18	47.35	95.92	18.64
Average error	24.79	23.27	66.27	8.35

where P_{L} is a polarization vector for Lorentz dispersion materials. After putting Eq. 5 into Eq. 4 we get

$$\nabla \times H = \varepsilon_0 \varepsilon_\infty \frac{\partial E}{\partial t} + \frac{\varepsilon_0 \partial P_{\text{L}}}{\partial t}. \tag{6}$$

The ADE approach is applied to Eq. 6 to simulate dispersive materials in time-domain forms [39], [50]. Now, we apply PSO to search for proper Lorentz parameters defining frequency-dependent dielectric constants of radiative cooling materials. We choose four representative radiative cooling materials (TiO_2 [44], Si_3N_4 [44], SiC [45], SiO_2 [46], [47]) in this work, although the proposed method can be applied to other dispersive materials.

The PSO is an evolutionary optimization algorithm that mimics the behavior of nature, such as ants and bees [29]. It iteratively finds a potential solution with moving particles that have social and cognitive factors. The number of dimensions of the PSO algorithm is the number of poles multiplied by three (ω_n, γ_n, and $\Delta\varepsilon_n$). The velocity of the particles is determined by

$$v_{\text{n}}^{\text{i+1}} = \omega \cdot v_{\text{n}}^{\text{i}} + C_1 \cdot \text{rand}() \cdot (\text{pBest}_{\text{n}}^{\text{i}} - x_{\text{n}}^{\text{i}}) + C_2 \cdot \text{rand}() \cdot (\text{gBest}_{\text{n}}^{\text{i}} - x_{\text{n}}^{\text{i}}), \tag{7}$$

where $v_{\text{n}}^{\text{i+1}}$ is a subsequent velocity of each particle in n_{th} dimension, which determines the next position of each particle in n_{th} dimension (x_{n}^{i}). ω is an inertia constant, and C_1 and C_2 are the cognitive and social constant, respectively, where both the cognitive and social constants are set to 2. rand() is a random number generation function, and pBest and gBest are a particle best position and a global best position found in the previous iterations. To evaluate the fitness of the particles, we define the figure of merit function ($\mathcal{F}$) as follow:

$$\zeta_{\Re} = \sum_\omega \frac{\Re[\varepsilon_{\text{Dat.}}(\omega) - \varepsilon_{\text{Lorentz}}(\omega)]}{\Re[\varepsilon_{\text{Lorentz}}(\omega) + \xi]} \tag{8}$$

$$\zeta_{\Im} = \sum_\omega \frac{\Im[\varepsilon_{\text{Dat.}}(\omega) - \varepsilon_{\text{Lorentz}}(\omega)]}{\Im[\varepsilon_{\text{Lorentz}}(\omega) + \xi]} \tag{9}$$

$$\mathcal{F} = \zeta_{\Re} + \zeta_{\Im}, \tag{10}$$

where ζ is a summation of error between frequency-dependent dielectric constants of the experimental data and Lorentz equation, and $\Re$, $\Im$ indicate the real and imaginary parts of the dielectric constants, respectively. Constant ξ is an additional parameter to prevent divergence of the figure-of-merit function when the permittivity of the data crosses zero. It has zero value for Si_3N_4 and SiC, while we gradually increase ξ for other materials until the fitting error is minimized. The PSO algorithm tries to minimize $\mathcal{F}$ by adjusting particles' velocities based on Eq. 7.

The number of Lorentz poles is first set to one; then, we gradually increase the number of the poles until the error ($\mathcal{F}$) satisfies a terminate condition. Increasing the number of Lorentz poles adds a computational burden [43] in the ADE-FDTD method [51] and escalates the complexity of the fitting problem. Therefore, we present our dielectric fitting results within five Lorentz poles, even though 10 to 15 poles demonstrate better accuracy. Table 1 shows

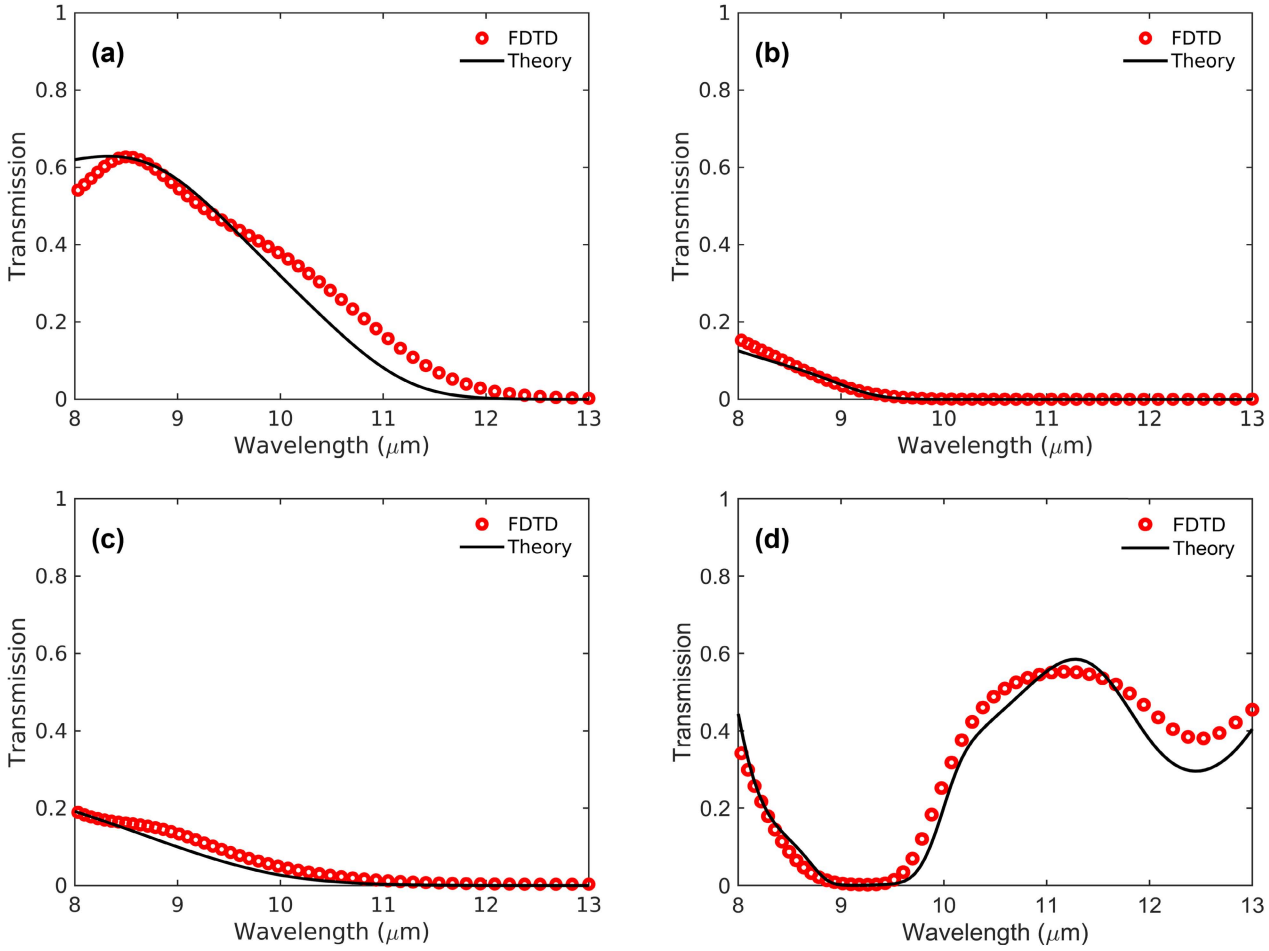


FIGURE 3. Transmission of dielectric slab on MIR spectrum. The red dots indicate dispersive FDTD simulation results using the optimized Lorentz parameters; the black curve indicates theoretical calculation based on transfer matrix method. (a) 5 μm thick TiO_2, (b) 5 μm thick Si_3N_4, (c) 5 μm thick SiC, (d) 2 μm thick SiO_2.

optimized Lorentz parameters for each material with four to five Lorentz poles. Figure 2 shows dispersion complex curve fitting [52] of radiative cooling materials, optimized by the PSO algorithm. The optimized Lorentz curves show minimal errors for TiO_2, Si_3N_4, and SiC while SiO_2 shows slight error on 9 μm and 10 μm in its real part. This can be improved further by employing 10 to 15 Lorentz poles; however, we limit our fitting up to five poles to make a consistent computational load. Plus, other experimental permittivity data for SiO_2 [44], [53], [54] demonstrate slightly different dielectric constants on 9 μm–10 μm; therefore, it might be unnecessary to overfitting one specific experimental data. We also compare the quality of our fitting against the most widely used evolutionary algorithms (Conventional Genetic Algorithm, Conventional Particle Swarm Optimization) as shown in Tab 2. We assume that the conventional PSO and the conventional GA algorithms have a figure of merit (F) given by $\mathcal{F} = \sum_{\omega} \frac{[\varepsilon_{\text{Dat.}}(\omega) - \varepsilon_{\text{Lorentz}}(\omega)]}{[\varepsilon_{\text{Lorentz}}(\omega)]}$.

III. FDTD ANALYSIS OF RADIATIVE COOLING MATERIALS

This section presents numerical examples to validate our dispersion curve fitting of the radiative cooling materials. We implement Lorentz parameters to MEEP [48], open-source FDTD solver, and simulate with a finite thickness of the dielectric slab. The FDTD time step is assigned by $\Delta t = C_n \Delta s / c_0$ where C_n is a courant number with values between 0 to 1, ΔS is a spatial step size, which is often called a grid spacing, and c_0 is a speed of light.

We use $\Delta s = \lambda_{\min}/50$ and $C_n = 0.5$. 5-μm and 2-μm-thick of the dielectric slabs are simulated with the FDTD method as shown in Fig. 3. Transmission of the incidence wave is calculated by accumulating the Fourier-transformed electric and magnetic fields for all points in the flux plane through the summation up to n_{th} discrete time step:

$$\tilde{f}(\omega) = \frac{1}{\sqrt{2\pi}} \sum_{n} e^{j\omega n \Delta t} f(n\Delta t) \Delta t \approx \frac{1}{\sqrt{2\pi}} \int e^{j\omega t} f(t)\, \mathrm{d}t, \tag{11}$$

where $\tilde{f}(\omega)$ is a Fourier transformed field, Δt is the FDTD time step, and $f(t)$ is a time-domain field. At the end of the simulation, these Fourier-transformed fields are used to

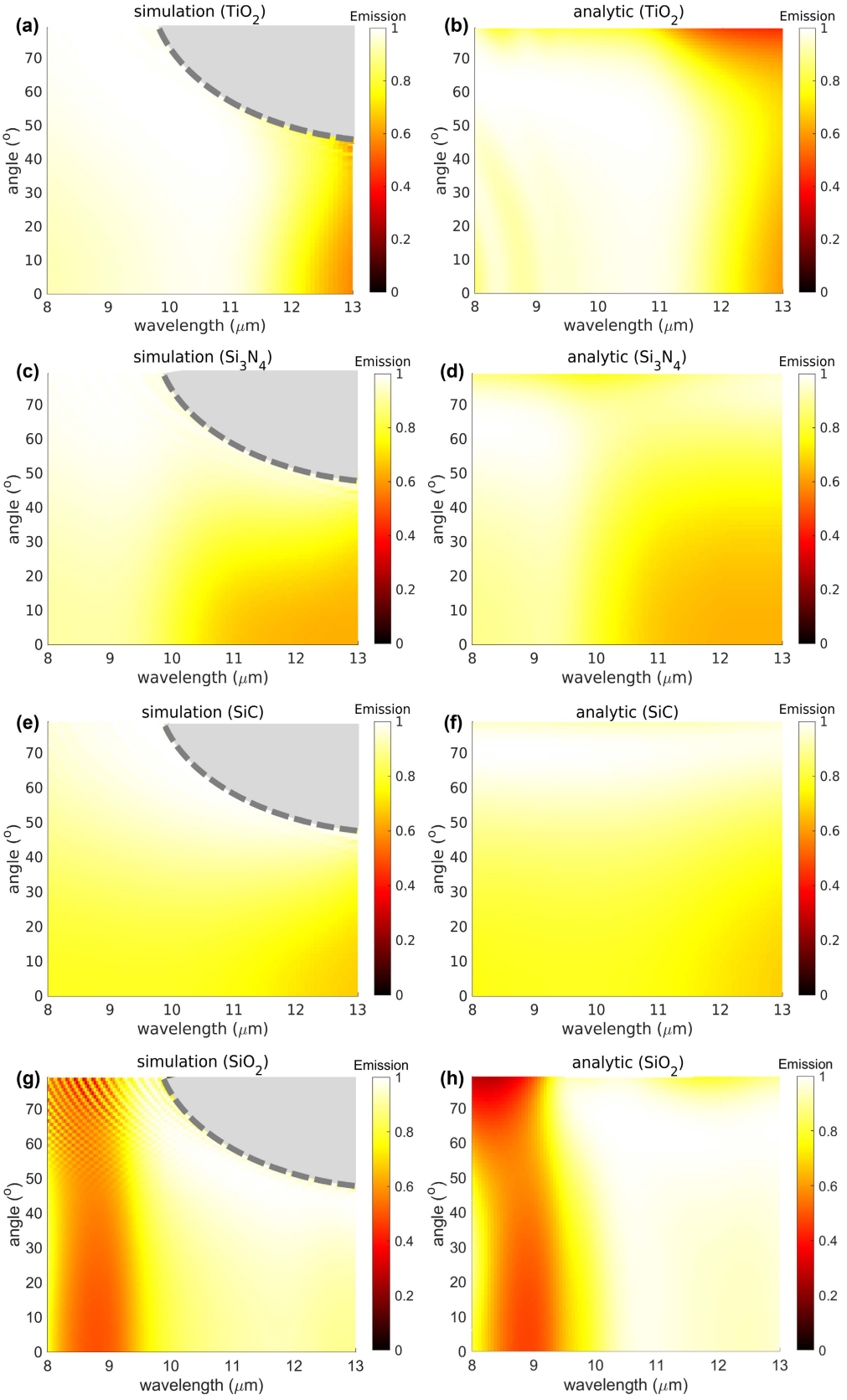


FIGURE 4. Incident angle-dependent MIR emission spectra of 20 μm thick dispersive materials. TiO_2 (a), Si_3N_4 (c), SiC (e), SiO_2 (g) indicate dispersive FDTD simulation results while TiO_2 (b), Si_3N_4 (d), SiC (f), SiO_2 (h) indicates analytic calculation based on the transfer matrix method.

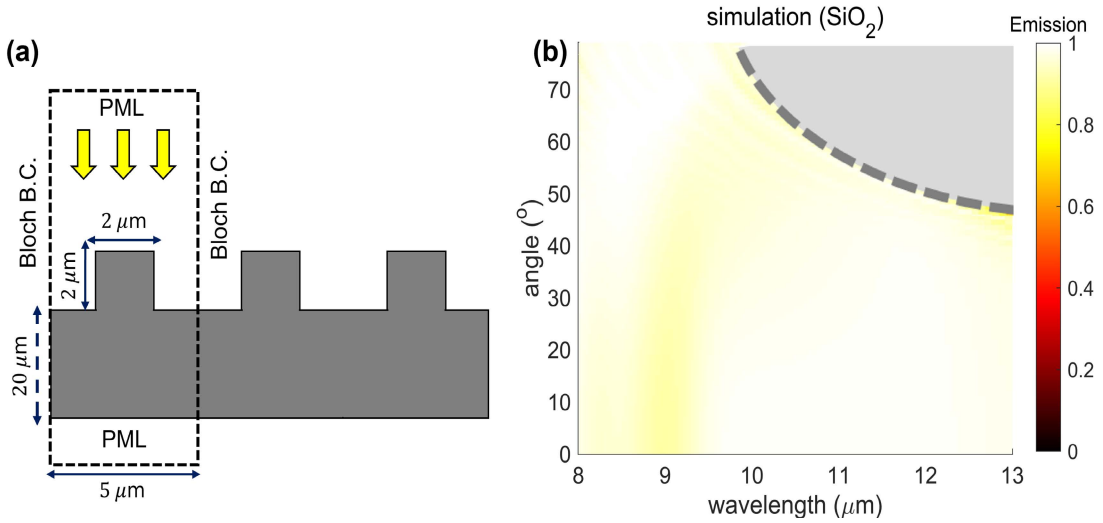


FIGURE 5. (a) SiO_2-based grating structure. (b) Incident angle-dependent MIR emission spectra of SiO_2 grating structure. 8.0–9.5μm wavelength emissivity is greatly improved compared with a planar SiO_2 structure.

compute the integral of the Poynting vectors to produce frequency-dependent transmission.

The red dots indicate Fourier-transformed FDTD simulation results, while the black curves indicate theoretical calculation based on TMM [19]. Analytic transmission through TMM can be calculated by

$$\mathrm{T} = \frac{1}{\mathbf{S}_{11}} = \frac{\mathbf{E}^+}{\mathbf{E}^+_0}, \tag{12}$$

where

$$\mathbf{S} = \begin{bmatrix} \mathbf{S}_{11} & \mathbf{S}_{12} \\ \mathbf{S}_{21} & \mathbf{S}_{22} \end{bmatrix}, \tag{13}$$

in Eq. 12, $\mathbf{E}^+_0$ is the global electric field, and $\mathbf{E}^+$ is the transmitted electric field. In Eq. 13, $\mathbf{S}$ is the global scattering matrix. Note that there is a slight error on the transmission of the TiO_2 dielectric slab shown in Fig. 3(a). This error can be improved with 10 Lorentz poles.

To understand emissivity of radiative cooling materials, one may need to calculate angle-dependent absorptivity of the materials. Then, we can apply Kirchhoff's law, which states that, for a body in equilibrium, the emissivity is equal to the absorptivity at each frequency and polarization [55]–[57]. Alternative methods utilize uncorrelated white-noise sources [55], [58] or trace formulation [59] to Maxwell's equation. In this work, we employ Kirchhoff's reciprocity to calculate the emissivity of the radiative cooling materials. The incidence planewave is excited at the top of the dielectric slabs, while transmission and reflection monitors are placed on both sides. Then, the absorptivity can be calculated via $\mathrm{A} = 1 - \mathrm{T} - \mathrm{R}$. Kirchhoff's law states that absorptivity for an incidence planewave with a specific angle equals the emissivity to that angle. Now, to analyze angle-dependent emissivity over the MIR regime, we excite a Bloch boundary planewave with different wavenumbers ($k = 2\pi/\lambda$) where $k = \sqrt{k_x^2 + k_y^2}$ in two dimensions. The Bloch boundary only supports a single wavenumber for each dimension (e.g., k_x, k_y); thus, a single FDTD simulation with the specific Bloch boundary condition corresponds to different incidence angles at different frequencies.

Angle(θ)-dependent emissivity is shown in Fig. 4. We use TMM for an angle-dependent analytic calculation of the emissivity, as shown in Fig. 4(b,d,f,h). The simulated emissivity is calculated via oblique incident Bloch boundary planewaves (total 81 simulations) and then interpolated to generate surface plots shown in Fig. 4(a,c,e,g). The simulated angle-dependent emissivity matches the analytic calculations with less than 1% root mean square error. Note that the gray area shown in the simulated emissivity plots is not calculated because it requires a high-angle and a greater wavenumber, where both of them increase a required k_x, which can exceed the wavenumber (k), meaning the nonpropagating mode. This can be simulated by adjusting the center wavelength of the planewave source.

A dielectric slab of SiO_2 shows low emissivity in the 8.0 to 9.5μm wavelength range due to high reflectivity and the low absorption coefficient. To further improve the emission characteristic of SiO_2, we design a 2D grating structure, as shown in Fig. 5(a). The grating or texturing structure improves the light coupling of thermal emission [33], decreasing reflection while redistributing the angular emission profile. Figure 5(a) shows a simulation structure, which includes 2-μm size SiO_2 based grating. As shown in Fig. 5(b), the simulated broadband angle-dependent emission shows that 8.0 to 9.5μm wavelength emissivity is greatly improved compared with a planar SiO_2 structure shown in Fig. 4(g). The angle-dependent emissivity shown in this work provides a pathway to accurately model and engineer novel micro/nanostructures for radiative cooling studies. Thus, we believe that this result can be applied to developing advanced radiative cooling strategies. For a realization of

this structure, one can use a holographic technique with a mode-locked Ti:sapphire laser [60] or utilize a commercially available SiO_2 grating product.

IV. CONCLUSION

We have modeled dispersive media used in radiative cooling applications for FDTD simulations. The PSO method is used to determine multipole Lorentz parameters for TiO_2, Si_3N_4, SiC, SiO_2 materials. Four to five Lorentz poles are used for modeling radiative cooling materials. Then, the modeling results are validated against theoretical calculations based on the transfer matrix method. Then, multiple FDTD simulations predict the angle-dependent broadband response of the radiative cooling materials. Finally, we simulate the SiO_2 grating structure to improve a planar SiO_2 emissivity. The proposed dispersion model may provide a path to efficiently discover an advanced radiative cooling structure.

REFERENCES

[1] W. Wu, S. Lin, M. Wei, J. Huang, H. Xu, Y. Lu, and W. Song, "Flexible passive radiative cooling inspired by Saharan silver ants," *Sol. Energy Mater. Sol. Cells*, vol. 210, Jun. 2020, Art. no. 110512.

[2] S. Jeong, C. Tso, Y. Wong, and C. Y. Chao, "FDTD simulations inspired by the daytime passive radiative cooling of the Sahara silver ant," in *Proc. 4th Int. Conf. Building Energy Environ.*, Melbourne, VIC, Australia, 2018, pp. 1–6.

[3] B.-Y. Liu, C.-H. Xue, H.-M. Zhong, X.-J. Guo, H.-D. Wang, H.-G. Li, M.-M. Du, M.-C. Huang, R.-X. Wei, L.-G. Song, B. Chang, and Z. Wang, "Multi-bioinspired self-cleaning energy-free cooling coatings," *J. Mater. Chem. A*, vol. 9, no. 43, pp. 24276–24282, 2021.

[4] M. Al-Nimr, M. Tahat, and M. Al-Rashdan, "A night cold storage system enhanced by radiative cooling—A modified Australian cooling system," *Appl. Thermal Eng.*, vol. 19, no. 9, pp. 1013–1026, 1999.

[5] T. Li, Y. Zhai, S. He, W. Gan, Z. Wei, M. Heidarinejad, D. Dalgo, R. Mi, X. Zhao, J. Song, J. Dai, C. Chen, A. Aili, A. Vellore, A. Martini, R. Yang, J. Srebric, X. Yin, and L. Hu, "A radiative cooling structural material," *Science*, vol. 364, no. 6442, pp. 760–763, 2019.

[6] M. Santamouris and D. Kolokotsa, "Passive cooling dissipation techniques for buildings and other structures: The state of the art," *Energy Buildings*, vol. 57, pp. 74–94, Feb. 2013.

[7] Y. Zhai, Y. Ma, S. N. David, D. Zhao, R. Lou, G. Tan, R. Yang, and X. Yin, "Scalable-manufactured randomized glass-polymer hybrid metamaterial for daytime radiative cooling," *Science*, vol. 355, no. 6329, pp. 1062–1066, Mar. 2017.

[8] M. M. Hossain, B. Jia, and M. Gu, "A metamaterial emitter for highly efficient radiative cooling," *Adv. Opt. Mater.*, vol. 3, no. 8, pp. 1047–1051, Aug. 2015.

[9] B. Ko, D. Lee, T. Badloe, and J. Rho, "Metamaterial-based radiative cooling: Towards energy-free all-day cooling," *Energies*, vol. 12, no. 1, p. 89, Dec. 2018.

[10] M. G. Meir, J. B. Rekstad, and O. M. Løvvik, "A study of a polymer-based radiative cooling system," *Sol. Energy*, vol. 73, no. 6, pp. 403–417, Dec. 2002.

[11] J. Mandal, Y. Fu, A. C. Overvig, M. Jia, K. Sun, N. N. Shi, H. Zhou, X. Xiao, N. Yu, and Y. Yang, "Hierarchically porous polymer coatings for highly efficient passive daytime radiative cooling," *Science*, vol. 362, no. 6412, pp. 315–319, Oct. 2018.

[12] E. Rephaeli, A. Raman, and S. Fan, "Ultrabroadband photonic structures to achieve high-performance daytime radiative cooling," *Nano Lett.*, vol. 13, no. 4, pp. 1457–1461, Apr. 2013.

[13] S. Atiganyanun, J. B. Plumley, S. J. Han, K. Hsu, J. Cytrynbaum, T. L. Peng, S. M. Han, and S. E. Han, "Effective radiative cooling by paint-format microsphere-based photonic random media," *ACS Photon.*, vol. 5, no. 4, pp. 1181–1187, Apr. 2018.

[14] L. Zhu, A. P. Raman, and S. Fan, "Radiative cooling of solar absorbers using a visibly transparent photonic crystal thermal blackbody," *Proc. Nat. Acad. Sci. USA*, vol. 112, no. 40, pp. 12282–12287, Oct. 2015.

[15] W. Li, Y. Li, and K. W. Shah, "A materials perspective on radiative cooling structures for buildings," *Sol. Energy*, vol. 207, pp. 247–269, Sep. 2020.

[16] A. Hervé, J. Drévillon, Y. Ezzahri, and K. Joulain, "Radiative cooling by tailoring surfaces with microstructures: Association of a grating and a multi-layer structure," *J. Quant. Spectrosc. Radiat. Transf.*, vol. 221, pp. 155–163, Dec. 2018.

[17] S.-R. Wu, K.-L. Lai, and C.-M. Wang, "Passive temperature control based on a phase change metasurface," *Sci. Rep.*, vol. 8, no. 1, pp. 1–6, Dec. 2018.

[18] S. Edalatpour and M. Francoeur, "Near-field radiative heat transfer between arbitrarily shaped objects and a surface," *Phys. Rev. B, Condens. Matter*, vol. 94, no. 4, Jul. 2016, Art. no. 045406.

[19] L. A. A. Pettersson, L. S. Roman, and O. Inganäs, "Modeling photocurrent action spectra of photovoltaic devices based on organic thin films," *J. Appl. Phys.*, vol. 86, no. 1, pp. 487–496, 1999.

[20] Y. Huang, M. Pu, Z. Zhao, X. Li, X. Ma, and X. Luo, "Broadband metamaterial as an 'invisible' radiative cooling coat," *Opt. Commun.*, vol. 407, pp. 204–207, Jan. 2018.

[21] J. Feng and M. Santamouris, "Numerical techniques for electromagnetic simulation of daytime radiative cooling: A review," *AIMS Mater. Sci.*, vol. 6, p. 1049, Oct. 2019.

[22] A. Taflove, S. C. Hagness, and M. Piket-May, "Computational electromagnetics: The finite-difference time-domain method," in *The Electrical Engineering Handbook*, vol. 3. Amsterdam, The Netherlands: Elsevier, 2005.

[23] D. Wu, C. Liu, Z. Xu, Y. Liu, Z. Yu, L. Yu, L. Chen, R. Li, R. Ma, and H. Ye, "The design of ultra-broadband selective near-perfect absorber based on photonic structures to achieve near-ideal daytime radiative cooling," *Mater. Des.*, vol. 139, pp. 104–111, Feb. 2018.

[24] H. H. Zhang, W. E. I. Sha, Z. X. Huang, and G. M. Shi, "Flexible and accurate simulation of radiation cooling with FETD method," *Sci. Rep.*, vol. 8, no. 1, pp. 1–10, Dec. 2018.

[25] H. Bao, C. Yan, B. Wang, X. Fang, C. Y. Zhao, and X. Ruan, "Double-layer nanoparticle-based coatings for efficient terrestrial radiative cooling," *Sol. Energy Mater. Sol. Cells*, vol. 168, pp. 78–84, Aug. 2017.

[26] T. J. Smy, S. A. Stewart, J. G. N. Rahmeier, and S. Gupta, "FDTD simulation of dispersive metasurfaces with Lorentzian surface susceptibilities," *IEEE Access*, vol. 8, pp. 83027–83040, 2020.

[27] H. Zheng, Y. Wu, K. Zhang, L. Wang, M. Wang, and E. Li, "Wide-band modeling on-chip spiral inductors using frequency-dependent conformal ADI-FDTD method," *IEEE Access*, vol. 7, pp. 184940–184949, 2019.

[28] H. Choi, Y.-H. Kim, J.-W. Baek, and K.-Y. Jung, "Accurate and efficient finite-difference time-domain simulation compared with CCPR model for complex dispersive media," *IEEE Access*, vol. 7, pp. 160498–160505, 2019.

[29] J. Robinson and Y. Rahmat-Samii, "Particle swarm optimization in electromagnetics," *IEEE Trans. Antennas Propag.*, vol. 52, no. 2, pp. 397–407, Feb. 2004.

[30] M. R. Sierra and C. A. C. Coello, "Improving PSO-based multi-objective optimization using crowding, mutation and ∈-dominance," in *Proc. Int. Conf. Evol. Multi-Criterion Optim.* Berlin, Germany: Springer, 2005, pp. 505–519.

[31] F. Marini and B. Walczak, "Particle swarm optimization (PSO). A tutorial," *Chemometrics Intell. Lab. Syst.*, vol. 149, pp. 153–165, Dec. 2015.

[32] M. I. Marković and A. D. Rakić, "Determination of optical properties of aluminium including electron reradiation in the lorentz-drude model," *Opt. Laser Technol.*, vol. 22, no. 6, pp. 394–398, Dec. 1990.

[33] H. Chung, K.-Y. Jung, X. T. Tee, and P. Bermel, "Time domain simulation of tandem silicon solar cells with optimal textured light trapping enabled by the quadratic complex rational function," *Opt. Exp.*, vol. 22, no. S3, pp. A818–A832, 2014.

[34] J. Park and K.-Y. Jung, "Numerical stability of modified Lorentz FDTD unified from various dispersion models," *Opt. Exp.*, vol. 29, no. 14, pp. 21639–21654, 2021.

[35] S.-G. Ha, J. Cho, J. Choi, H. Kim, and K.-Y. Jung, "FDTD dispersive modeling of human tissues based on quadratic complex rational function," *IEEE Trans. Antennas Propag.*, vol. 61, no. 2, pp. 996–999, Feb. 2013.

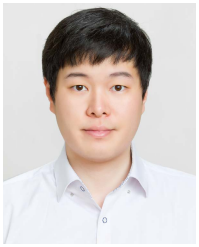
[36] J. Cho, S.-G. Ha, Y. B. Park, H. Kim, and K.-Y. Jung, "On the numerical stability of finite-difference time-domain for wave propagation in dispersive media using quadratic complex rational function," *Electromagnetics*, vol. 34, no. 8, pp. 625–632, Nov. 2014.

[37] H. Chung, J. Cho, S.-G. Ha, S. Ju, and K.-Y. Jung, "Accurate FDTD dispersive modeling for concrete materials," *ETRI J.*, vol. 35, no. 5, pp. 915–918, Oct. 2013.

[38] P. Markos and C. M. Soukoulis, *Wave Propagation*. Princeton, NJ, USA: Princeton Univ. Press, 2008.
[39] H. Choi, J.-W. Baek, and K.-Y. Jung, "Comprehensive study on numerical aspects of modified Lorentz model-based dispersive FDTD formulations," *IEEE Trans. Antennas Propag.*, vol. 67, no. 12, pp. 7643–7648, Dec. 2019.
[40] K. P. Prokopidis and D. C. Zografopoulos, "Investigation of the stability of ADE-FDTD methods for modified Lorentz media," *IEEE Microw. Wireless Compon. Lett.*, vol. 24, no. 10, pp. 659–661, Oct. 2014.
[41] W. H. Weedon and C. M. Rappaport, "A general method for FDTD modeling of wave propagation in arbitrary frequency-dispersive media," *IEEE Trans. Antennas Propag.*, vol. 45, no. 3, pp. 401–410, Mar. 1997.
[42] R. Siushansian and J. LoVetri, "A comparison of numerical techniques for modeling electromagnetic dispersive media," *IEEE Microw. Guided Wave Lett.*, vol. 5, no. 12, pp. 426–428, Dec. 1995.
[43] M. Han, R. W. Duttonm, and S. Fan, "Model dispersive media in finite-difference time-domain method with complex-conjugate pole-residue pairs," *IEEE Microw. Wireless Compon. Lett.*, vol. 16, no. 3, pp. 119–121, Mar. 2006.
[44] J. Kischkat, S. Peters, B. Gruska, M. Semtsiv, M. Chashnikova, M. Klinkmüller, O. Fedosenko, S. Machulik, A. Aleksandrova, G. Monastyrskyi, Y. Flores, and W. T. Masselink, "Mid-infrared optical properties of thin films of aluminum oxide, titanium dioxide, silicon dioxide, aluminum nitride, and silicon nitride," *Appl. Opt.*, vol. 51, no. 28, pp. 6789–6798, 2012.
[45] J. I. Larruquert, A. P. Pérez-Marín, S. García-Cortés, L. Rodríguez-de-Marcos, J. A. Aznárez, and J. A. Méndez, "Self-consistent optical constants of sic thin films," *J. Opt. Soc. Amer. A, Opt. Image Sci.*, vol. 28, no. 11, pp. 2340–2345, 2011.
[46] R. Kitamura, L. Pilon, and M. Jonasz, "Optical constants of silica glass from extreme ultraviolet to far infrared at near room temperature," *Appl. Opt.*, vol. 46, no. 33, pp. 8118–8133, Nov. 2007.
[47] S. Popova, T. Tolstykh, and V. Vorobev, "Optical characteristics of amorphous quartz in the 1400–200 cm-1 region," *Opt. Spectrosc.*, vol. 33, pp. 444–445, 1972.
[48] A. F. Oskooi, D. Roundy, M. Ibanescu, P. Bermel, J. D. Joannopoulos, and S. G. Johnson, "Meep: A flexible free-software package for electromagnetic simulations by the FDTD method," *Comput. Phys. Commun.*, vol. 181, no. 3, pp. 687–702, 2010.
[49] D. Whitley, "A genetic algorithm tutorial," *Statist. Comput.*, vol. 4, no. 2, pp. 65–85, Jun. 1994.
[50] M. A. Alsunaidi and A. A. Al-Jabr, "A general ADE-FDTD algorithm for the simulation of dispersive structures," *IEEE Photon. Technol. Lett.*, vol. 21, no. 12, pp. 817–819, Jun. 15, 2009.
[51] Y.-J. Kim and K.-Y. Jung, "Accurate and efficient finite-difference time-domain formulation of dusty plasma," *IEEE Trans. Antennas Propag.*, vol. 69, no. 10, pp. 6600–6606, Oct. 2021.
[52] E. C. Levy, "Complex-curve fitting," *IRE Trans. Autom. Control*, vol. 4, no. 1, pp. 37–43, 1959.
[53] L. V. Rodríguez-de-Marcos, J. I. Larruquert, J. A. Méndez, and J. A. A. Aznárez, "Self-consistent optical constants of SiO_2 and Ta_2O_5 films," *Opt. Mater. Exp.*, vol. 6, no. 11, pp. 3622–3637, 2016.
[54] H. Philipp, "Silicon dioxide (SiO_2)(glass)," in *Handbook of Optical Constants of Solids*. Amsterdam, The Netherlands: Elsevier, 1997, pp. 749–763.
[55] C. Luo, A. Narayanaswamy, G. Chen, and J. D. Joannopoulos, "Thermal radiation from photonic crystals: A direct calculation," *Phys. Rev. Lett.*, vol. 93, no. 21, Nov. 2004, Art. no. 213905.
[56] D. L. C. Chan, M. Soljačić, and J. D. Joannopoulos, "Direct calculation of thermal emission for three-dimensionally periodic photonic crystal slabs," *Phys. Rev. E, Stat. Phys. Plasmas Fluids Relat. Interdiscip. Top.*, vol. 74, no. 3, Sep. 2006, Art. no. 036615.
[57] F. Reif, *Fundamentals of Statistical and Thermal Physics*. Long Grove, IL, USA: Waveland Press, 2009.
[58] A. W. Rodriguez, O. Ilic, P. Bermel, I. Celanovic, J. D. Joannopoulos, M. Soljačić, and S. G. Johnson, "Frequency-selective near-field radiative heat transfer between photonic crystal slabs: A computational approach for arbitrary geometries and materials," *Phys. Rev. Lett.*, vol. 107, no. 11, Sep. 2011, Art. no. 114302.
[59] W. Yao, F. Verdugo, R. E. Christiansen, and S. G. Johnson, "Trace formulation for photonic inverse design with incoherent sources," 2021, *arXiv:2111.13046*.
[60] K. Kawamura, T. Ogawa, N. Sarukura, M. Hirano, and H. Hosono, "Fabrication of surface relief gratings on transparent dielectric materials by two-beam holographic method using infrared femtosecond laser pulses," *Appl. Phys. B, Lasers Opt.*, vol. 71, no. 1, pp. 119–121, Jul. 2000.



MUNSEONG BAE received the B.S. degree in electrical engineering from Myongji University, Yongin-si, South Korea, in 2021. He is currently pursuing the M.S. degree in developing inverse design algorithm for novel metasurfaces with Soongsil University. His research interests include fast inverse design algorithm, deep learning, and metasurfaces.



HAEJUN CHUNG received the B.S. degree *(magna cum laude)* in electrical engineering from the Illinois Institute of Technology, Chicago, USA, in 2011, and from Hanyang University, Seoul, South Korea, in 2012, and the M.S. and Ph.D. degrees in electrical and computer engineering from Purdue University, IN, USA, in 2013 and 2017, respectively. He joined applied physics at Yale University, CT, USA, as a Postdoctoral Research Associate, in 2017. Then, he joined mechanical engineering at the Massachusetts Institute of Technology, MA, USA, as a Postdoctoral Research Associate, in 2020. He joined Soongsil University, Seoul, in 2021, where he is currently an Assistant Professor with the School of Electrical Engineering. His main research interests include fast inverse design algorithm, novel metasurfaces, metalenses, biosensors, and photovoltaics.